



HAL
open science

Mathematical Analysis and Calculation of Molecular Surfaces

Chaoyu Quan, Benjamin Stamm

► **To cite this version:**

Chaoyu Quan, Benjamin Stamm. Mathematical Analysis and Calculation of Molecular Surfaces. 2015.
hal-01205580v1

HAL Id: hal-01205580

<https://hal.sorbonne-universite.fr/hal-01205580v1>

Preprint submitted on 25 Sep 2015 (v1), last revised 18 Mar 2016 (v2)

HAL is a multi-disciplinary open access archive for the deposit and dissemination of scientific research documents, whether they are published or not. The documents may come from teaching and research institutions in France or abroad, or from public or private research centers.

L'archive ouverte pluridisciplinaire **HAL**, est destinée au dépôt et à la diffusion de documents scientifiques de niveau recherche, publiés ou non, émanant des établissements d'enseignement et de recherche français ou étrangers, des laboratoires publics ou privés.

Mathematical Analysis and Calculation of Molecular Surfaces

Chaoyu Quan, Benjamin Stamm

September 25, 2015

Abstract

In this article we derive a complete characterization of the Solvent Excluded Surface (SES) for molecular systems including a complete characterization of singularities of the surface. The proofs are constructive so that the theory allows for efficient algorithms in order to compute the area of the SES and the volume of the SES-cavity, or to visualize the surface. Further, we propose to refine the notion of SAS and SES in order to take inner holes in a solute molecule into account or not.

1 Introduction

The majority of chemically relevant reactions take place in the liquid phase and the effect of the environment (solvent) is important and should be considered in various chemical computations. In consequence, a continuum solvation model is a model in which the effect of the solvent molecules on the solute are described by a continuous model [20]. In continuum solvation continuum models, the notion of molecular cavity and molecular surface is a fundamental part of the model. The molecular cavity occupies the space of the solute molecule where a solvent molecule cannot be present and the molecular surface, the boundary of the corresponding cavity, builds the interface between the solute and the solvent respectively between the continuum and the atomistic description of the physical model. A precise understanding of the nature of the surface is therefore essential for the coupled model and in consequence for running numerical computations. The Van der Waals (VdW) surface, the Solvent Accessible Surface (SAS) and the Solvent Excluded Surface (SES) are well-established concepts. The VdW surface is more generally used in chemical calculations, such as in the recent developments [4, 13] for example, of numerical approximations to the COnductor-like Screening MOdel (COSMO) due to the simplicity of the cavity. Since the VdW surface is the topological boundary of the union of spheres, the geometric features are therefore easier to understand. However, the SES, which is considered to be a more precise description of the cavity, is more complicated and its analytical characterization remains unsatisfying despite a large number of contributions in literature.

1.1 Previous Work

In quantum chemistry, atoms of a molecule can be represented by VdW-balls with VdW-radii obtained from experiments [16]. The VdW surface of a solute molecule is consequently defined as the topological boundary of the union of all VdW-balls. For a given solute molecule, its SAS and the corresponding SES were first introduced by Lee & Richards in the 1970s [12, 17], where the solvent

molecules surrounding a solute molecule are reduced to spherical probes [20]. The SES is also called “the smooth molecular surface” or “the Connolly surface”, due to Connolly’s fundamental work [7]. He has divided the SES into three types of patches: convex spherical patches, saddle-shaped toroidal patches and concave spherical triangles. But the self-intersection among different patches in this division often causes singularities despite that the whole SES is smooth almost everywhere. This singularity problem has led to difficulty in many associated works with the SES, for example, failure of SES meshing algorithms and imprecise calculation of molecular areas or volumes, or has been circumvented by approximate techniques [6]. In 1996, Michel Sanner treated some special singularity cases in his MSMS (Michel Sanner’s Molecular Surface) software for meshing molecular surfaces [19]. However, to our knowledge, the complete characterization of the singularities of the SES remains unsolved.

1.2 Contribution

In this paper, we will characterize the above molecular surfaces with implicit functions, as well as provide explicit formulas to compute analytically the area of molecular surfaces and the volume of molecular cavities. We first propose a method to compute the signed distance function to the SAS, based on three equivalence statements which also induce a new partition of \mathbb{R}^3 . In consequence, a computable implicit function of the corresponding SES is given from the relatively simple relationship between the SES and the SAS. Furthermore, we will redefine different types of SES patches mathematically so that the singularities will be characterized explicitly. Besides, by applying the Gauss-Bonnet theorem [8] and the Gauss-Green theorem [10], we succeed to calculate analytically all the molecular areas and volumes, in particular for the SES. These quantities are thought to be useful in protein modeling, such as describing the hydration effects [18, 3].

In addition, we will refine the notion of SAS and SES by considering the possible inner holes in the solute molecule yielding the notions of the complete SAS (cSAS) and the corresponding complete SES (cSES). To distinguish them, we call respectively the previous SAS and the previous SES as the exterior SAS (eSAS) and the exterior SES (eSES). A method with binary tree to construct all these new molecular surfaces will also be proposed in this paper in order to provide a computationally efficient method.

1.3 Outline

We first introduce the concepts of implicit surfaces in the second section and the implicit functions of molecular surfaces are given in the third section. In the fourth section, we present two more precise definitions about the SAS, either by taking the inner holes of the solute molecule considered into account or not. Then, based on three equivalence statements that are developed, we propose a computable method to calculate the signed distance function from any point to the SAS analytically. In this process, a new Voronoi-type diagram for the SAS-cavity is given which allows us to calculate analytically the area of the SAS and the volume inside the SAS. In the fifth section, a computable implicit function of the SES is deduced directly from the signed distance function to the SAS and according to the new Voronoi-type diagram, all SES-singularities are characterized. Still within this section, the formulas of calculating the area of the SES and the volume inside the SES will be provided. In the sixth section, we explain how to construct the SAS (cSAS and eSAS) and the SES (cSES and eSES) for a given solute molecule considering the possible inner holes. In the last section, we provide some conclusions of this article.

2 Introduction to Implicit Surfaces

We start with presenting the definition of implicit surfaces [21]. In a very general context, a subset $\mathcal{O} \subset \mathbb{R}^n$ is called an *implicit object* if there exists a real-valued function $f : U \rightarrow \mathbb{R}^k$ with $\mathcal{O} \subset U \subset \mathbb{R}^n$, and a subset $V \subset \mathbb{R}^k$, such that $\mathcal{O} = f^{-1}(V)$. That is,

$$\mathcal{O} = \{p \in U : f(p) \in V\}.$$

The above definition of an implicit object is broad enough to include a large family of subsets of the space. In this paper, we consider the simple case where $U = \mathbb{R}^3$, $V = \{0\}$ and $f : \mathbb{R}^3 \rightarrow \mathbb{R}$ is a real-valued function. In consequence, an implicit object is represented as a zero-level set $\mathcal{O} = f^{-1}(0)$, which is also called an *implicit surface* in \mathbb{R}^3 , and the function f is called an *implicit function* of the implicit surface. Notice that there are various implicit functions to represent one surface in the form of a zero-level set.

The signed distance function f_S of a closed bounded oriented surface S in \mathbb{R}^3 , determines the distance from a given point $p \in \mathbb{R}^n$ to the surface S , with the sign determined by whether p lies inside S or not. That is to say,

$$f_S(p) = \begin{cases} -\inf_{x \in S} \|p - x\| & \text{if } p \text{ lies inside } S, \\ \inf_{x \in S} \|p - x\| & \text{if } p \text{ lies outside } S. \end{cases} \quad (2.1)$$

This is naturally an implicit function of S .

3 Implicit Molecular Surfaces

In quantum chemistry, atoms of a molecule are represented by VdW-balls with VdW radii which are experimentally fitted, given the underlying chemical element [16]. In consequence and mathematically speaking, the VdW surface is defined as the topological boundary of the union of all VdW-balls. Besides, the SAS of a solute molecule is defined by the center of an idealized spherical probe rolling over the solute molecule, that is, the surface enclosing the region in which the center of a spherical probe can not enter. Finally, the SES is defined by the same spherical probe rolling over the solute VdW-cavity, that is, the surface enclosing the region in which a spherical probe can access. In other words, the SES is the boundary of the union of all spherical probes that do not intersect the VdW-balls of the solute molecule, see Figure 1 for a graphical illustration.

We denote by M the number of atoms in a solute molecule, by $c_i \in \mathbb{R}^3$ and $r_i \in \mathbb{R}^+$ the center and the radius of the i -th VdW atom. The open ball with center c_i and radius r_i is called the i -th VdW-ball. The Van der Waals surface can consequently be represented as an implicit surface $f_{vdw}^{-1}(0)$ with the following implicit function:

$$f_{vdw}(p) = \min_{i=1,\dots,M} \{\|p - c_i\|_2 - r_i\}, \quad \forall p \in \mathbb{R}^3. \quad (3.2)$$

Similarly, the open ball with center c_i and radius $r_i + r_p$ is called the i -th SAS-ball denoted by B_i , where r_p is the radius of the idealized spherical probe. Furthermore, we denote by S_i the i -th SAS-sphere corresponding to B_i , that is, $S_i = \partial B_i$. Similar to the VdW surface, the SAS can be represented as an implicit surface $\tilde{f}_{sas}^{-1}(0)$ with the following implicit function:

$$\tilde{f}_{sas}(p) = f_{vdw}(p) - r_p = \min_{i=1,\dots,M} \{\|p - c_i\|_2 - r_i - r_p\}, \quad \forall p \in \mathbb{R}^3. \quad (3.3)$$

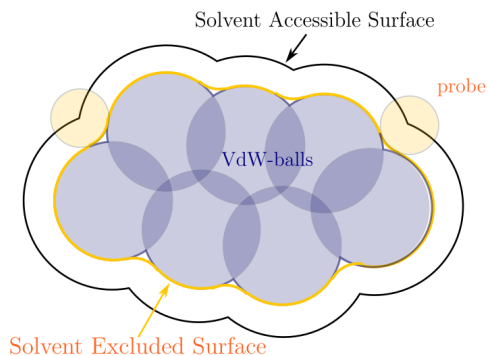


Figure 1: This is a 2-dimension (2D) schematics of the Solvent Accessible Surface and the Solvent Excluded Surface, both defined by a spherical probe in orange rolling over the molecule atoms in dark blue.

We notice that the above implicit function of the SAS is simple to compute. It seems nevertheless hopeless to us to further obtain an implicit function of the SES if constructing upon this simple implicit function $\tilde{f}_{sas}(p)$ which is not a distance function. On the other hand, having the signed distance function, see (2.1), at hand would allow the construction of an implicit function for the SES due to the geometrical relationship between the SAS and the SES.

Indeed, according to the fact that any point on the SES has signed distance $-r_p$ to the SAS, an implicit function of the SES is obtained directly as:

$$f_{ses}(p) = f_{sas}(p) + r_p, \quad (3.4)$$

which motivates the choice of using the signed distance function to represent the SAS. From the above formula, the SES can be represented by a level set $f_{sas}^{-1}(-r_p)$, associated with the signed distance function f_{sas} to the SAS. Therefore, the key point becomes how to compute the signed distance $f_{sas}(p)$ from a point $p \in \mathbb{R}^3$ to the SAS. Generally speaking, given a general surface $S \subset \mathbb{R}^3$ and any arbitrary point $p \in \mathbb{R}^3$, it is difficult to compute the signed distance from p to S . However, considering that the SAS is a special surface formed by the union of SAS-spheres, this computation can be done analytically.

We state a remark about another implicit function to characterize the SES, proposed by Pomelli and Tomasi [15]. In [14], this function can be written as:

$$\tilde{f}_{ses}(p) = \min_{1 \leq i < j < k \leq M} f_{ijk}(p), \quad \forall p \in \mathbb{R}^3, \quad (3.5)$$

where f_{ijk} represents the signed distance function to the SES of the i -th, j -th and k -th VdW atom. However, this representation might fail sometimes, see two representative 2D examples in Figure 2. Indeed, the formula (3.5) for each molecule in Figure 2 can be rewritten as:

$$\tilde{f}_{ses}(p) = \min_{1 \leq i < j \leq 3} f_{i,j}(p), \quad \forall p \in \mathbb{R}^2, \quad (3.6)$$

where $f_{i,j}$ represents the signed distance function to the SES of the i -th and the j -th VdW atom. However, each molecular cavity defined by $\{p \in \mathbb{R}^2 : \tilde{f}_{ses}(p) \leq 0\}$ has excluded the region in grey inside the real SES.

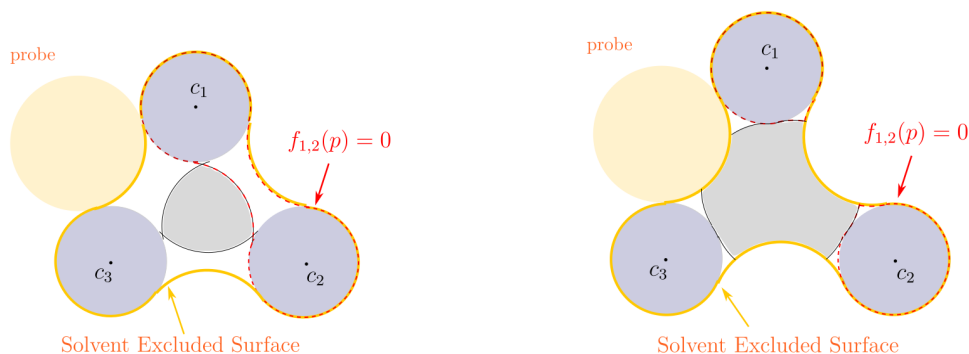


Figure 2: The above figures illustrate two SESs of two artificial molecules respectively containing three atoms. In each of them, $f_{1,2}$ denotes the signed distance function to the SES of the 1-th and the 2-th atoms which is depicted with dashed red curves ($f_{2,3}$ and $f_{1,3}$ are similar).

Further, the region enclosed by the Van der Waals surface is called the VdW-cavity, that is, any point p in the VdW-cavity satisfies $f_{vdw}(p) \leq 0$. More generally, we call the region enclosed by a molecular surface as the corresponding molecular cavity. In consequence, the region enclosed by the SAS is called the SAS-cavity, and the region enclosed by the SES is called the SES-cavity. Similarly, any point p in the SAS-cavity satisfies $f_{sas}(p) \leq 0$, and any point p in the SES-cavity satisfies $f_{ses}(p) \leq 0$.

4 The Solvent Accessible Surface

In the framework of continuum solvation models, using the VdW-cavity as the solvent molecular cavity has the characteristic that its definition does not depend in any way on characteristics of the solvent. In other words, the above-mentioned VdW surface has ignored the size and shape of the solvent molecules, while the definition of the Solvent Accessible Surface includes some of these characteristics. In the following, we first provide two more precise mathematical definitions of the SAS considering possible inner holes of a solute molecule. After that, we will provide a formula for the signed distance function to the SAS, which is indeed based on three equivalence statements, providing explicitly a closest point on the SAS to any point in \mathbb{R}^3 . In this process, a new Voronoi-type diagram will be proposed to make a partition of the space \mathbb{R}^3 , which, in turn, will also be used to calculate the exact volume of the SAS-cavity.

4.1 Mathematical Definitions

In [12], the Solvent Accessible Surface is defined by the set of the centers of the spherical probe when rolling over the VdW surface of the molecule. At first glance, one could think that it can equivalently be seen as the topological boundary of the union of all SAS-balls of the molecule. However, we notice that there might exist some inner holes inside the molecules where a solvent molecule can not be present. In consequence, the SAS may or may not be composed of several separate surfaces, see Figure 3 for a graphical illustration. This inspires us to propose two more precise surfaces: the **complete Solvent Accessible Surface** (cSAS) defined simply as the boundary of of

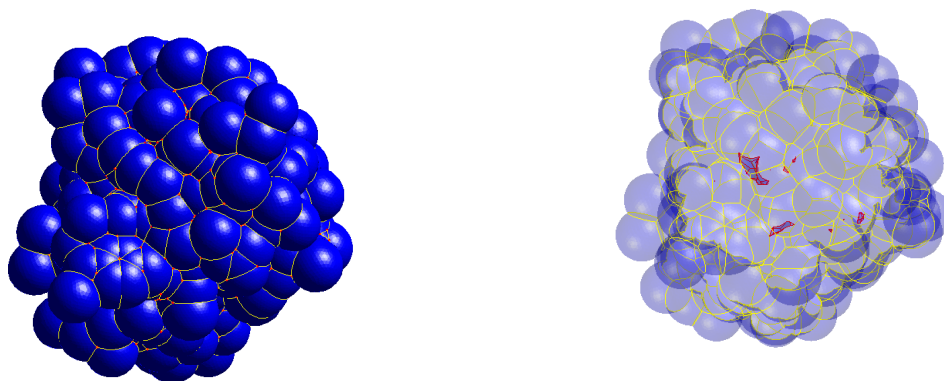


Figure 3: The left figure shows the components of the eSAS of the protein 1B17 (the probe radius $r_p = 1.2\text{\AA}$): open spherical patches in blue, open circular arcs in yellow and intersection points in red. The right figure shows the exterior surface (transparent) and the interior surfaces of the eSES of the protein 1B17. The boundary of an exterior spherical patch of the eSAS is composed of circular arcs depicted in yellow, and the boundary of an interior spherical patch of the cSAS is composed of circular arcs depicted in purple.

the union of the SAS-balls, and the **exterior Solvent Accessible Surface** (eSAS) defined as the outmost surface obtained when a probe rolls over the exterior of the molecule, see Figure 4. In the case where there are no interior holes inside the molecule, the cSAS and the eSAS will coincide. We make a convention that the SAS refers to both the cSAS and the eSAS in a general context.

Since both the cSAS and the eSAS are two closed sets, there exists a closest point on the SAS to any given point $p \in \mathbb{R}^3$, which is denoted by x_{sas}^p . Thus, the signed distance function f_{sas} can be written as:

$$f_{sas}(p) = \begin{cases} -\|p - x_{sas}^p\| & \text{if } p \text{ lies inside the SAS,} \\ \|p - x_{sas}^p\| & \text{if } p \text{ lies outside the SAS.} \end{cases} \quad (4.7)$$

In the above formula, x_{sas}^p depends on p . When p lies on the SAS, p coincides with x_{sas}^p and $f_{sas}(p) = 0$. It remains therefore to find a closest point x_{sas}^p on the SAS to the given point $p \in \mathbb{R}^3$. Note that there might exist more than one closest point on the SAS to the point p and x_{sas}^p is chosen as one of them. In the context, this is not an easy task. In the following, for the particular case of the SAS, we propose a way to calculate analytically a closest point on the SAS to a given point p , based on three equivalence statements.

4.2 Equivalence Statements

According to the definitions of the cSAS and the eSAS, these two molecular surfaces are both composed of three types of parts: open spherical patches, open circular arcs and intersection points (formed by the intersection of at least three SAS-spheres), see Figure 3. Note that an SAS intersection point can in theory be formed by the intersection of more than three SAS-spheres. However,

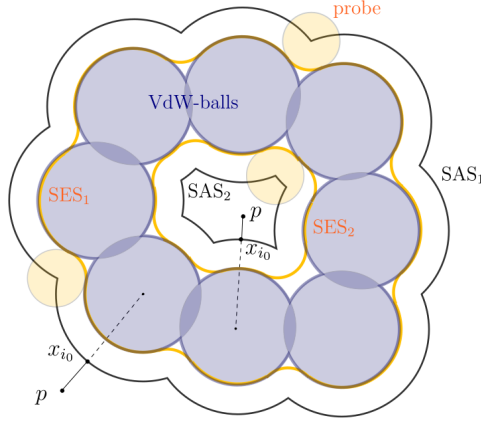


Figure 4: This is a 2D schematic of different molecular surfaces, including the VdW surface, the cSAS, the eSAS, the cSES and the eSES. The yellow discs denote the probes, representing solvent molecules, while the blue discs denote the VdW-balls. SAS_1 is the trace of the probe center when a probe rolls over the exterior of the VdW-balls, while SAS_2 is the trace of the probe center when a probe rolls over the inner holes of the VdW-balls. SES_1 and SES_2 respectively denote the corresponding solvent excluded surfaces to SAS_1 and SAS_2 . The cSAS is the union of SAS_1 and SAS_2 , while the eSAS is just SAS_1 . Similarly, the cSES is the union of SES_1 and SES_2 , while the eSES is just SES_1 . Finally, x_{i_0} is a closest point on the SAS to a given point p .

these cases can be divided into multiple triplets of SAS-spheres for simplicity as mentioned in [11]. In this spirit, we make an assumption that all SAS intersection points are formed by the intersection of three SAS-spheres. Furthermore, we assume that any SAS-ball is not included by any other (otherwise, the inner SAS-ball can be ignored) In the following analysis.

For an SAS, denote by m_1 the number of the SAS spherical patches, by m_2 the number of the SAS circular arcs, and by m_3 the number of the SAS intersection points. Then, denote by P_m the m -th SAS spherical patch on the SAS where $m = 1, \dots, m_1$. Denote by l_m the m -th SAS circular arc on the SAS where $m = 1, \dots, m_2$. Denote by x_m the m -th SAS intersection point on the SAS where $m = 1, \dots, m_3$. Furthermore, denote by I the set of all SAS intersection points written as:

$$I = \{x_m : m = 1, \dots, m_3\} = \{x \in SAS : \exists 1 \leq i < j < k \leq M, \text{ s.t. } x \in S_i \cap S_j \cap S_k\}.$$

With the above notations, we consider to calculate a closest point on the SAS to a given point p in the case when p lies outside the SAS (the cSAS or the eSAS).

Lemma 4.1. *Let the point p lie outside the SAS (the cSAS or the eSAS), i.e. $\|p - c_i\| \geq r_i + r_p, \forall 1 \leq i \leq M$. Further, let $i_0 \in \{1, \dots, M\}$ be such that*

$$\|p - c_{i_0}\| - (r_{i_0} + r_p) = \min_{1 \leq i \leq M} \{\|p - c_i\| - (r_i + r_p)\}. \quad (4.8)$$

Then, the point

$$x_{i_0} = c_{i_0} + (r_{i_0} + r_p) \frac{p - c_{i_0}}{\|p - c_{i_0}\|}, \quad (4.9)$$

is the closest point to p on the SAS and

$$f_{sas}(p) = \|p - x_{i_0}\| = \min_{1 \leq i \leq M} \{\|p - c_i\| - (r_i + r_p)\}. \quad (4.10)$$

Proof. The proof involves basic geometric manipulations and is left to the reader. \square

So far, we have discussed the case when p lies outside the SAS (both the cSAS and the eSAS), which is not too difficult to deal with. Next, we need to consider the case where p lies inside the (complete or exterior) SAS-cavity, to obtain the signed distance function $f_{sas}(p)$ from any point $p \in \mathbb{R}^3$ to the SAS. The following analysis can be applied to both the cSAS and the eSAS. This problem is handled inversely, in the sense that we will determine the region in the molecular cavity for an arbitrary given point $x_{sas} \in \text{SAS}$, such that x_{sas} is a closest point to any point in this region. To do this, we first define a mapping $R : X \mapsto Y$, where X is a subset of the SAS, and $Y = R(X)$ is the region in the SAS-cavity, such that there exists a closest point in X on the SAS to any point in Y . That is,

$$Y = \{y : y \text{ lies in the SAS-cavity and } \exists x_{sas}^y \in X \text{ s.t. } x_{sas}^y \text{ is a closest point to } y\}.$$

In the following, we propose three equivalence statements between a point x_{sas} on the SAS and the corresponding region $R(x_{sas})$ for three cases where x_{sas} lies respectively on the three different types of the SAS. We recall first, however, a useful inequality between two signed distance functions to two surfaces.

Proposition 4.1. *Consider two bounded, closed and oriented surfaces $S \subset \mathbb{R}^3$ and $S' \subset \mathbb{R}^3$ with two corresponding signed distance functions $f_S(p)$ and $f_{S'}(p)$. If the cavity inside S is contained in the cavity inside S' , then we have $f_{S'}(p) \leq f_S(p)$, $\forall p \in \mathbb{R}^3$.*

With the above proposition, we propose first a result which connects a point on an SAS spherical patch with a closed line segment in the SAS-cavity.

Theorem 4.1. *Assume that $p \in \mathbb{R}^3$ is a point in the SAS-cavity and x_{sas} is a point on the SAS. If x_{sas} is on an SAS spherical patch P_m on the i -th SAS-ball S_i , then x_{sas} is a closest point on the SAS to p if and only if p lies on the closed line segment $[c_i, x_{sas}]$. That is, $R(x_{sas}) = [c_i, x_{sas}]$. Further, the closest point x_{sas} on the SAS is unique if and only if $p \neq c_i$. If $p = c_i$, then any point on P_m is a closest point to p .*

Proof. First suppose that x_{sas} is a closest point to p with $x_{sas} \in P_m \subset S_i$. Since P_m is an open set, take a small enough neighborhood V of x_{sas} such that $V \subset P_m$, see Figure 5, and since x_{sas} is a closest point on the SAS to p , we have

$$\|p - x_{sas}\| \leq \|p - x\|, \quad \forall x \in V, \quad (4.11)$$

which yields that the vector from x_{sas} to p is perpendicular to any vector in the tangent plane of S_i at x_{sas} , thus the vector from p to x_{sas} is the normal vector at x_{sas} of S_i . In consequence, p must lie on the line passing through x_{sas} and the center c_i of S_i . Furthermore, from the convexity of P_m , p has to lie on the closed line segment $[c_i, x_{sas}]$.

On the other hand, suppose that $x_{sas} \in P_m \subset S_i$, and $p \in [c_i, x_{sas}]$. In consequence, x_{sas} is obviously a closest point on the sphere S_i to p , see Figure 5. The signed distance function $f_{S_i}(p)$ is equal to $-\|p - x_{sas}\|$. Notice that the cavity inside S_i , i.e. B_i , is contained in the

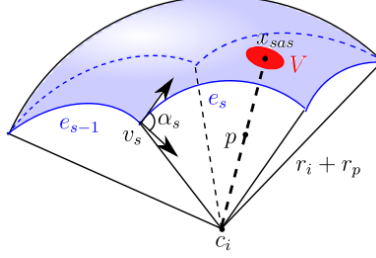


Figure 5: Illustration when the point x_{sas} lies on an SAS spherical patch P_m which is part of an SAS-sphere S_i , and p lies on the segment $[c_i, x_{sas}]$. V represents a neighborhood of x_{sas} on the spherical patch. α_s is the angle variation at the vertex v_s between two neighboring circular arcs e_{s-1} and e_s on the boundary of this spherical patch.

SAS-cavity. We can then use Proposition 4.1 by taking S as S_i and S' as the SAS, to obtain $f_{sas}(p) \leq f_{S_i}(p) = -\|p - x_{sas}\|$. Therefore, we have

$$-\|p - x\| \leq f_{sas}(p) \leq -\|p - x_{sas}\|, \quad \forall x \in \text{SAS}. \quad (4.12)$$

That is, $\|p - x\| \geq \|p - x_{sas}\|$, $\forall x \in \text{SAS}$, which means that x_{sas} is a closest point on the SAS to p .

Finally, assume that $p \in [c_i, x_{sas}]$. If $p = c_i$, then any point on P_m is a closest point to p because the distance is uniformly $\|c_i - x_{sas}\| = r_i + r_p$. If $p \neq c_i$, then the open ball $B_r(p)$ with $r = \|p - x_{sas}\| < r_i + r_p$ is included in B_i and $\partial B_r(p) \cap S_i = \{x_{sas}\}$, which implies that x_{sas} is the unique closest point to p . \square

Next, we propose another equivalence statement, which connects a point on an SAS circular arc with a closed triangle in the SAS-cavity.

Theorem 4.2. *Assume that $p \in \mathbb{R}^3$ is a point in the SAS-cavity and x_{sas} is a point on the SAS. If x_{sas} is on an SAS circular arc l_m associated with S_i and S_j , then x_{sas} is a closest point on the SAS to p if and only if p lies in the closed triangle $\Delta x_{sas}c_i c_j$ defined by three vertices x_{sas} , c_i and c_j . That is, $R(x_{sas}) = \Delta x_{sas}c_i c_j$. Further, the closest point x_{sas} on the SAS is unique if and only if p does not belong to the edge $[c_i, c_j]$. If $p \in [c_i, c_j]$, any point on l_m is a closest point to p .*

Proof. First suppose that x_{sas} is a closest point to p with $x_{sas} \in l_m \subset S_i \cap S_j$. Since l_m is an open circle arc on the circle $S_i \cap S_j$, take a small enough neighboring curve γ_0 of x_{sas} with $\gamma_0 \subset l_m$, see Figure 6. Since x_{sas} is a closest point to p , we have

$$\|p - x_{sas}\| \leq \|p - x\|, \quad \forall x \in \gamma_0. \quad (4.13)$$

Denote by p' the projection of p onto the plane where l_m lies. By substituting $\|p - x_{sas}\|^2 = \|p - p'\|^2 + \|p' - x_{sas}\|^2$ and $\|p - x\|^2 = \|p - p'\|^2 + \|p' - x\|^2$ into the inequality (4.13), we obtain that

$$\|p' - x_{sas}\| \leq \|p' - x\|, \quad \forall x \in \gamma_0, \quad (4.14)$$

which yields that the vector from x_{sas} to p' is perpendicular to the tangent vector of γ_0 at x_{sas} . In consequence, p' has to lie on the ray Ox_{sas} starting from O and passing through x_{sas} , where O is the center of the circular arc l_m . Thus, p must lie on the closed half plane Π defined by the

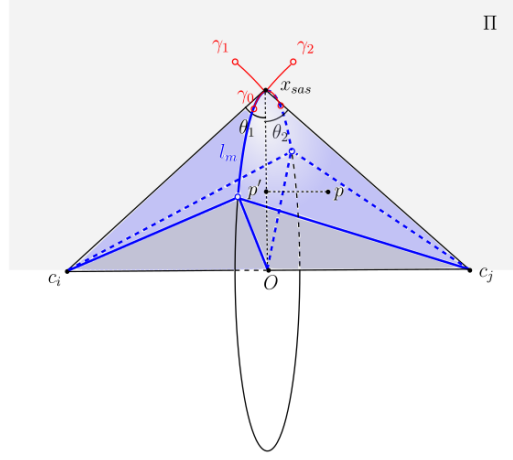


Figure 6: Illustration when l_m is an SAS circular arc associated with two SAS-spheres S_i and S_j . The point x_{sas} on l_m is a closest point on the SAS to p . γ_0 is a small neighborhood of x_{sas} on the circular arc l_m , whereas γ_1 and γ_2 represent two small neighboring curves of x_{sas} on the SAS, with x_{sas} as the endpoints, $\gamma_1 \subset \Pi \cap S_i \cap \text{SAS}$, and $\gamma_2 \subset \Pi \cap S_j \cap \text{SAS}$.

three points x_{sas} , c_i and c_j and whose boarder is the line passing through c_i and c_j . The closed half plane Π contains the ray Ox_{sas} and is perpendicular to the plane where l_m lies. We then take another two neighboring curves γ_1 and γ_2 of x_{sas} , with $\gamma_1 \subset \Pi \cap S_i \cap \text{SAS}$ and $\gamma_2 \subset \Pi \cap S_j \cap \text{SAS}$, see Figure 6. In this case, γ_1 has one closest endpoint x_{sas} and is open at the other end, which is the same for γ_2 . From the assumption that x_{sas} is a closest point on the SAS to p , we have the following inequality

$$\|p - x_{sas}\| \leq \|p - x\|, \quad \forall x \in \gamma_1 \cup \gamma_2. \quad (4.15)$$

This yields that $p \in \Delta x_{sas}c_i c_j$, where $\Delta x_{sas}c_i c_j$ is the closed triangle on Π with three vertices x_{sas} , c_i and c_j . Otherwise, we can find a point $x \in (\gamma_1 \cup \gamma_2) \setminus x_{sas}$ strictly closer to p than x_{sas} , which contradicts the assumption.

On the other hand, suppose that $p \in \Delta x_{sas}c_i c_j$. In consequence, it is not difficult to obtain that x_{sas} is the closest point to p on $\partial(B_i \cup B_j)$, where B_i and B_j are the corresponding SAS-balls corresponding to S_i and S_j as mentioned above. Similarly, we know that the signed distance function $f_{\partial(B_i \cup B_j)}(p)$ is equal to $-\|p - x_{sas}\|$, and notice that $B_i \cup B_j$ is contained in the SAS-cavity. We can use again Proposition 4.1, by taking S as $\partial(B_i \cup B_j)$ and S' as the SAS, to obtain $f_{sas}(p) \leq f_{\partial(B_i \cup B_j)}(p) = -\|p - x_{sas}\|$. Therefore, we have

$$-\|p - x\| \leq f_{sas}(p) \leq -\|p - x_{sas}\|, \quad \forall x \in \text{SAS}. \quad (4.16)$$

That is, $\|p - x\| \geq \|p - x_{sas}\|$, $\forall x \in \text{SAS}$, which means that x_{sas} is a closest point on the SAS to p .

If $p \in [c_i, c_j]$, then any point on l_m is a closest point to p since the distance from any point on l_m to p is constant. If $p \in \Delta x_{sas}c_i c_j \setminus [c_i, c_j]$, then the open ball $B_r(p)$ with $r = \|p - x_{sas}\| < r_i + r_p$ is included in $B_i \cup B_j$ and $\partial B_r(p) \cap \partial(B_i \cup B_j) = \{x_{sas}\}$, which implies that x_{sas} is the unique closest point to p . \square

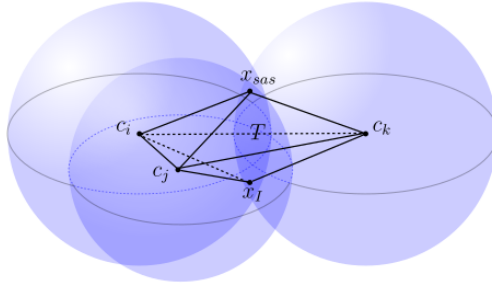


Figure 7: This figure illustrates the closed region T of three SAS-spheres with the centers (c_i, c_j, c_k) , where the tetrahedron T has five vertices $(x_{sas}, c_i, c_j, c_k, x_I)$. Here, x_{sas} is one SAS intersection point in I , and x_I is the other SAS intersection point.

By mapping with R a whole SAS spherical patch P_m to the SAS-cavity, we obtain a spherical sector $R(P_m)$ in the SAS-cavity with cap P_m , center c_i and radius $r_i + r_p$, see Figure 5. Similarly, by mapping with R a whole SAS circular arc l_m to the SAS-cavity, we obtain a double-cone region $R(l_m)$ in the SAS-cavity with the circular sector corresponding to l_m as base, c_i and c_j as vertices, see Figure 6.

Removing now the above-mentioned spherical sectors and double-cone regions from the SAS-cavity, the closed hull of the remaining region, denoted by T , is consequently a collection of closed separate polyhedrons, see an example of three atoms in Figure 7. Each polyhedron is denoted by T_n with index n and thus $T = \bigcup T_n$. Considering now the last case where x_{sas} is an SAS intersection point x_m , we have a third equivalence statement as a corollary of the previous two equivalence statements.

Corollary 4.1. *If x_{sas} is an SAS intersection point $x_m \in I$ associated with S_i , S_j and S_k , then x_{sas} is a closest point on the SAS to p if and only if p lies in the closed region T and x_{sas} is a closest point in I to p .*

In other words, for an arbitrary intersection point $x_m \in I$, we have the formula of its corresponding region in the SAS-cavity as following:

$$R(x_m) = T \cap \{p : \|p - x_m\| \leq \|p - x\|, \forall x \neq x_m, x \in I\}. \quad (4.17)$$

It is not difficult to find that $R(x_m)$ is a closed polyhedron. At the same time, mapping I into the SAS-cavity with R , we obtain $R(I) = T$.

With the three equivalence statements as well as the above-defined map R , we obtain in fact a non-overlapping decomposition of the SAS-cavity, including spherical sectors, double-cone regions and polyhedrons. It should be emphasized that given a point $p \in \mathbb{R}^3$ contained in the SAS-cavity and known the region where p lies, we can then calculate a closest point x_{sas}^p on the SAS to p according to this decomposition. The signed distance function $f_{sas}(p)$ can therefore be calculated analytically by the formula 4.7, which, in turn, will ultimately provide an implicit function of the SES. In the next subsection, we will investigate further in the partition of the SAS-cavity based on the above equivalence statements, in order to compute efficiently the area of the SAS and the volume of the SAS-cavity.

4.3 New Voronoi-type Diagram

The above non-overlapping decomposition of the SAS-cavity can also be seen as a new Voronoi-type diagram, which will be presented comparing with the well-known Voronoi Diagram and the Power Diagram recalled in the following.

a. Voronoi Diagram

The Voronoi diagram [9] was initially a partition of a 2D plane into regions based on the distance to points in a specific subset of the plane. In the general case, for an Euclidean subspace $X \subset \mathbb{R}^n$ endowed with a distance function d and a tuple of nonempty subsets $(A_i)_{i \in K}$ in X , the Voronoi region R_i associated with A_i is the set of all points in X whose distance to A_i is not greater than their distance to any other set A_j for $j \neq i$. In other words, with the distance function between a point x and a set A_i defined as

$$d_V(x, A_i) = \inf_{y \in A_i} \{d(x, y) \mid y \in A_i\},$$

the formula of the Voronoi region R_i is then given by:

$$R_i = \{x \in X \mid d_V(x, A_i) \leq d_V(x, A_j), \forall j \neq i\}. \quad (4.18)$$

Most commonly, each subset A_i is taken as a point and its corresponding Voronoi region R_i is consequently a polyhedron, see an example of three points in \mathbb{R}^2 in Figure 8.

b. Power Diagram

In computational geometry, the power diagram [1], also called the Laguerre-Voronoi diagram, is another partition of a 2D plane into polygonal cells defined from a set of circles in \mathbb{R}^2 . In the general case, for a set of circles $(C_i)_{i \in K}$ (or spheres) in \mathbb{R}^n with $n \geq 2$, the power region R_i associated with C_i consists of all points whose power distance to C_i is not greater than their power distance to any other circle C_j , for $j \neq i$. The the power distance from a point x to a circle C_i with center c_i and radius r_i is defined as

$$d_P(x, C_k) = \|x - c_k\|^2 - r_k^2,$$

the formula of the Power region R_i is then given by:

$$R_i = \{x \in \mathbb{R}^n \mid d_P(x, C_i) \leq d_P(x, C_j), \forall j \neq i\}.$$

The power diagram is a form of generalized Voronoi diagram, in the sense that you can take the circles C_i instead of the centers c_i and simply replace the distance function d_V in the Voronoi diagram with the power distance function d_P , to obtain the power diagram, see an example of three circles in \mathbb{R}^2 in Figure 8. Notice that the power distance is not a real distance function. By summing up the volume of each power region inside the SAS-cavity, one can calculate the exact volume of the cSAS-cavity, which is equivalent to calculate the volume of the union of balls, see [2, 5].

c. New Voronoi-Type Diagram

In this paper, we propose a new Voronoi-type diagram for a set of spheres in \mathbb{R}^3 (or circles in \mathbb{R}^2), which is inspired by the non-overlapping decomposition of the SAS-cavity. We will see that this new diagram allows to calculate exactly not only the volume of the (complete or exterior) SAS-cavity, but also the (complete or exterior) SES-cavity which will be defined in the next section.

We first look at the new Voronoi-type diagram for a set of discs in the case of 2D. Notice that the boundary γ of the union of these discs can be classified into two types: open circular arcs $\{l_1, l_2, \dots, l_n\}$ and intersection points $\{x_1, x_2, \dots, x_n\}$, with the number of circular arcs equal to the number of intersection points. Take $A_1 = l_1, \dots, A_n = l_n, A_{n+1} = \{x_1, x_2, \dots, x_n\}$ in the Voronoi diagram. In consequence, we obtain $n + 1$ corresponding new Voronoi-type regions $\{R_1, \dots, R_n, R_{n+1}\}$, where R_i is given by (4.18).

From a similar mapping R and similar equivalence theorems, we know that the part of R_i inside γ is a circular sector when $1 \leq i \leq n$, and R_{n+1} is the remaining region composed of polygons, see an example of three circles in Figure 8. For any point $x \in \mathbb{R}^2$, we have $x \in R_i$ if and only if there exists a point in A_i such that it is a closet point to x on γ .

In the 3D case, the SAS consists of three types of geometrical quantities: open spherical patches, open circular arcs and intersection points. Similarly to the case in 2D, we take $A_1 = P_1, \dots, A_{m_1} = P_{m_1}, A_{m_1+1} = l_1, \dots, A_{m_1+m_2} = l_{m_2}$ and $A_{m_1+m_2+1} = \{x_1, \dots, x_{m_3}\}$ with the above-mentioned notations. In consequence, we obtain $m_1 + m_2 + 1$ corresponding new Voronoi-type regions $\{R_1, \dots, R_{m_1}, R_{m_1+1}, \dots, R_{m_1+m_2}, R_{m_1+m_2+1}\}$.

With the mapping R defined in the last section, we know that the spherical sector $R(P_m)$ corresponds to R_m in the SAS-cavity, the double-cone region $R(l_m)$ corresponds to R_{m_1+m} in the SAS-cavity, and the closed region $R(I)$ coincides with $R_{m_1+m_2+1}$. For any point $x \in \mathbb{R}^3$, we have $x \in R_i$ if and only if there exists a point in A_i such that it is a closet point on the SAS to x . The new Voronoi-type diagram is a powerful tool for calculating analytically the molecular area and volume, which is a direct consequence of the three equivalence statements. Given the components of the SAS, the new Voronoi-type diagram can be obtained directly according to the three equivalence statements, while the power diagram needs more complicated computations.

4.4 SAS-Area and SAS-Volume

In this paper, the area of the SAS is called the SAS-area and the volume of the SAS-cavity is called the SAS-volume. Similarly, the area of the SES is called the SES-area and the volume of the SES-cavity is called the SES-volume. Next, we will use the Gauss-Bonnet theorem of differential geometry to calculate the SAS-area, and then will use the new Voronoi-type diagram to calculate the SAS-volume.

a. SAS-Area

To calculate analytically the solvent accessible area, the Gauss-Bonnet theorem has already been applied in the 1980s [7], which allows one to calculate the area of each SAS spherical patch with the information along its boundary, and then sum them up. We introduce briefly the key formula used in this calculation to keep the article complete. The area of a spherical patch P can be obtained from the Gauss-Bonnet theorem as following (see Figure 5):

$$\sum_i \alpha_i + \sum_i k_{e_i} |e_i| + \frac{1}{r^2} A_P = 2\pi\chi, \quad (4.19)$$

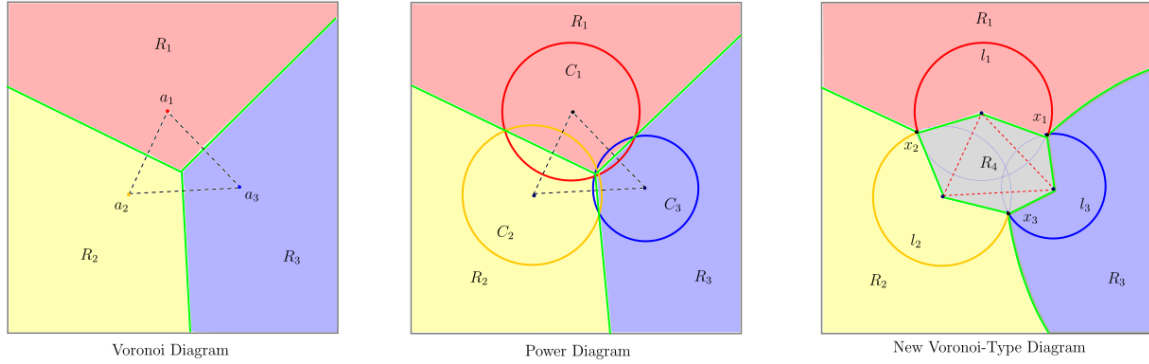


Figure 8: The left figure gives the Voronoi diagram of three points $\{a_1, a_2, a_3\}$ in \mathbb{R}^2 . R_1 is the Voronoi region associated with a_1 , while R_2 associated with a_2 and R_3 associated with a_3 . The middle figure gives the power diagram of three circles $\{C_1, C_2, C_3\}$ in \mathbb{R}^2 , with three corresponding power regions R_1, R_2 and R_3 . The right figure gives the new Voronoi-type diagram of three circles in \mathbb{R}^2 , with four regions R_1, R_2, R_3 and R_4 respectively corresponding to l_1, l_2, l_3 and $\{x_1, x_2, x_3\}$.

where α_i is the angle at the vertex v_i on the boundary between two neighboring circular arcs e_{i-1} and e_i , k_{e_i} is the geodesic curvature of the edge e_i , $|e_i|$ is the length of this edge e_i and A_P is the area of the patch P . Finally, χ is the Euler characteristic of P , which is equal to 2 minus the number of loops forming the boundary of P . Through the above formula, we calculate the area of each SAS spherical patch A_{P_m} and sum them up to get the SAS-area A_{sas} :

$$A_{sas} = \sum_{m=1}^{m_1} A_{P_m}. \quad (4.20)$$

b. SAS-Volume

In the new Voronoi-type diagram, the SAS-cavity is decomposed into three types of region: spherical sectors, double-cone regions and polyhedrons. For a spherical patch P_m on S_i with center c_i and radius $r_i + r_p$, the volume of the corresponding spherical sector $R(P_m)$, denoted by V_{P_m} , can be calculated as following:

$$V_{P_m} = \frac{1}{3} A_{P_m} (r_i + r_p).$$

For a circular arc l_m associated with S_i and S_j (see Figure 6), the volume of the corresponding double-cone region $R(l_m)$, denoted by V_{l_m} , can be calculated as following:

$$V_{l_m} = \frac{1}{6} r_{l_m} |l_m| \|c_i - c_j\|.$$

where r_{l_m} is the radius of this circular arc and $|l_m|$ is the length of l_m . Finally, the volume of the closed region $T = R(I)$ can be calculated according the Gauss-Green theorem [10]:

$$V_T = \sum_t A_t (n_t \cdot n_0),$$

where t denotes a triangle on the boundary of T , A_t is the area of the triangle t , n_t is the outward pointing normal vector of t and n_0 is an arbitrary given unit direction vector in \mathbb{R}^3 , for example, $n_0 = (1, 0, 0)$.

From the above three formulas, we sum up the volume of each spherical sector, each double-cone region and the polyhedron T , to get the solvent accessible volume V_{sas} as below:

$$V_{sas} = \frac{1}{3} \sum_{m=1}^{m_1} A_{P_m} (r_i + r_p) + \frac{1}{6} \sum_{m=1}^{m_2} r_{l_m} |l_m| \|c_i - c_j\| + \sum_t A_t (n_t \cdot n_0).$$

5 The Solvent Excluded Surface

The Solvent Excluded Surface was first proposed by Lee & Richards in the 1970s [17]. Although the SES is believed to give a more accurate description of the molecular cavity, it is more complicated than the other two molecular surfaces. We first give two more precise definitions of the SES considering inner holes of a molecule. After that, we define mathematically different types of patches on the SES, which helps us to characterize and calculate analytically singularities on the SES. Finally, combining the above-proposed new Voronoi-type diagram and the upcoming singularity analysis, we calculate the exact SES-area and the SES-volume.

5.1 Mathematical Definitions

In previous works [12, 17], the SES is defined as the topological boundary of the union of all possible spherical probes that do not intersect any VdW atom of the molecule. In other words, the SES is the boundary of the cavity where a spherical probe can never be present. However, there might exist inner holes inside the solute molecule. Similar to the definitions of the cSAS and the eSAS, the **complete Solvent Excluded Surface** (cSES) is defined as the set of all points with signed distance $-r_p$ to the cSAS, while the **exterior Solvent Excluded Surface** (eSES) is defined as the set of all points with signed distance $-r_p$ to the eSAS. We make a similar convention as before that the SES refers to both the cSES and the eSES. From the geometrical relationship between the SAS and the SES, i.e. $SES = f_{sas}^{-1}(r_p)$, we propose an implicit function of the SES:

$$f_{ses}(p) = \begin{cases} -\|p - x_{sas}^p\| + r_p & \text{if } f_{sas}(p) \leq 0, \\ \|p - x_{sas}^p\| + r_p & \text{if } f_{sas}(p) \geq 0, \end{cases} \quad (5.21)$$

where x_{sas}^p is a closest point on the SAS to p , which depends on p and can be obtained directly from the equivalence statements.

In Connolly's work [7], the SES is divided into three types of patches: convex spherical patches, saddle-shaped toroidal patches and concave spherical triangles, see Figure 9. The convex spherical patches are the remainders of VdW-spheres, which occur when the probe is rolling over the surface of an atom and touches no other atom. The toroidal patches are formed when the probe is in contact with two atoms at the same time and rotates around the axis connecting the centers of these two atoms. While rolling, the probe traces out small circular arcs on each of the two VdW-spheres, which build the boundaries between the convex spherical patches and the toroidal patches. The concave spherical triangles occur if the probe is simultaneously in contact with more than or equal to three VdW-spheres. Here, the probe is in a fixed position, meaning that it is centered at an SAS intersection point and cannot roll without losing contact to at least one of the atoms.

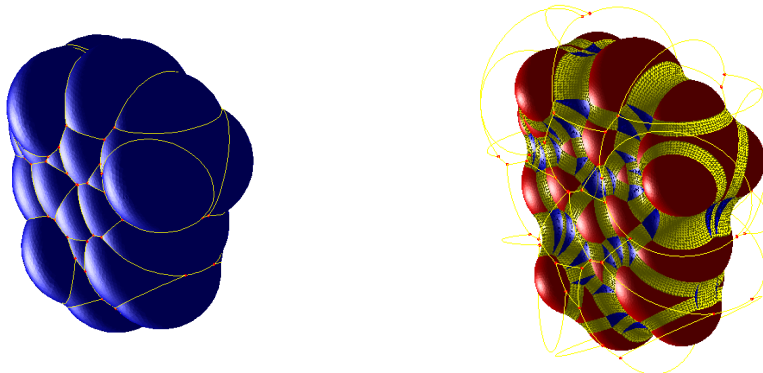


Figure 9: The above figures show both the SAS and the SES of the caffeine molecule (the probe radius $r_p = 1.2\text{\AA}$). On the left, the SAS is composed of spherical patches in blue, circular arcs in yellow and intersection points in red. On the right, the patches in red (resp. in yellow or in blue) are the corresponding convex spherical patches (resp. toroidal patches or concave spherical patches) on the SES.

The intersection between different SES patches might occur which leads to singularities on the SES, referred to as SES-singularities, see Figure 10. Despite some particular cases which have been studied by Sanner [19], a characterization of these singularities is not known. We will provide a complete characterization, using the above equivalence statements as well as the following analysis of the SES-singularities. To start with, we give three new definitions of different SES patches from the mathematical point of view:

- 1) **Convex Spherical Patch:** A convex spherical patch on the SES, denoted by P_+ , is defined as the set of the points on the SES such that there exists a closest point on the SAS belonging to a common SAS spherical patch P_m , where $1 \leq m \leq m_1$.
- 2) **Toroidal Patch:** A toroidal patch on the SES, denoted by P_t , is defined as the set of the points on the SES such that there exists a closest point on the SAS belonging to a common SAS circular arc l_m , where $1 \leq m \leq m_2$.
- 3) **Concave Spherical Patch:** A concave spherical patch on the SES, denoted by P_- , is defined as the set of the points on the SES such that there exists a common SAS intersection point x_m which is a closest point on the SAS to each point on P_- , where $1 \leq m \leq m_3$.

According to these new definitions, the three types of patches can be rewritten mathematically as follows:

$$\begin{cases} P_+ = \{p : f_{ses}(p) = 0, p \in R(P_m)\}, & 1 \leq m \leq m_1 \\ P_t = \{p : f_{ses}(p) = 0, p \in R(l_m)\}, & 1 \leq m \leq m_2 \\ P_- = \{p : f_{ses}(p) = 0, p \in R(x_m)\}, & 1 \leq m \leq m_3 \end{cases} \quad (5.22)$$

where f_{ses} is the implicit function of the SES and R is the mapping defined in the previous section. Actually, a convex spherical patch and a toroidal patch are defined in the same way as Connolly,

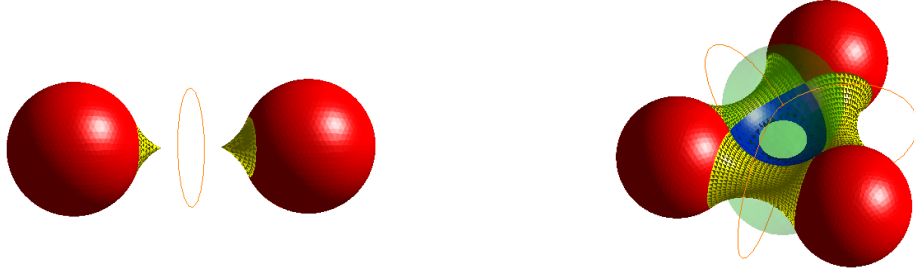


Figure 10: The above figures show two kinds of singularities respectively on a toroidal patch P_t and on a concave spherical patch P_- . On the left, each of the two point-singularities (cusps) on the toroidal patch P_t has an infinite number of closest points on the corresponding SAS circle in orange. On the right, the SES-singularities on the concave spherical patch P_- form a singular circle. The two spherical spheres in green center at two SAS intersection points in red.

while a new-defined concave patch might not be triangle-shaped because its new definition takes into account the intersection among different SES patches. The above new definitions of the SES patches ensure that different SES patches will not intersect with each other, for the reason that different patches belong to different new Voronoi-type regions in the new Voronoi-type diagram.

5.2 SES-Singularities

Before characterizing the singularities on the SES, it is necessary to recall the properties of the signed distance function f_S to a surface S in \mathbb{R}^n ($n \geq 1$) as below:

- 1) f_S is differentiable almost everywhere, and it satisfies the Eikonal Equation: $|\nabla f_S| = 1$.
- 2) If f_S is differentiable at a point $p \in \mathbb{R}^n$, then there exists a small neighborhood V of p such that f_S is differentiable in V .
- 3) For any point $p \in \mathbb{R}^n$, f_S is non-differentiable at p if and only if the number of the closest points on S to p is greater than or equal to 2.

We call a point $x_{ses} \in SES$ a *singularity* if the SES is not smooth at x_{ses} , which means that its implicit function $f_{ses}(p) = f_{sas}(p) + r_p$ is non-differentiable at x_{ses} in \mathbb{R}^3 . If $x_{ses} \in SES$ is a singularity, we obtain consequently that f_{sas} is non-differentiable at x_{ses} . From the last property above, we therefore can characterize the SES-singularities by the following equivalence.

Corollary 5.1. *A point $x_{ses} \in SES$ is a singularity if and only if the number of the closest points on the SAS to x_{ses} is greater than or equal to 2.*

We now investigate the different types of singularities that can appear on each of the three patch types. From the definitions of different SES patches, it is relatively easy to calculate the convex spherical patches and the toroidal patches given the components of the SAS. In the following, we illustrate how to calculate P_- exactly, which provides therefore a complete characterization of the

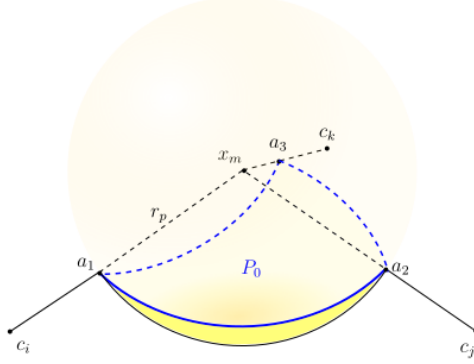


Figure 11: This is the schematic of the concave spherical triangle P_0 corresponding to an intersection point x_m , with the boundary composed of three circular arcs in blue ($\widehat{a_1a_2}$, $\widehat{a_2a_3}$ and $\widehat{a_3a_1}$) on the spherical probe. This spherical triangle touches at the same time three VdW-balls at vertices (a_1, a_2, a_3) .

SES-singularities later. Denote by P_0 the concave spherical triangle ($P_- \subset P_0$) corresponding to an SAS intersection point x_m showed in Figure 11 and by K the set of all intersection points in I with distances less than $2r_p$ to x_m , that is,

$$K = \{x \in I : \|x - x_m\| < 2r_p, x \neq x_m\},$$

so that K collects all SAS intersection points "near" x_m . According to the definition of P_- corresponding to x_m and the equation (4.17), we have the following formula:

$$P_- = P_0 \cap R(x_m) = P_0 \cap T \cap \{p : \|p - x_m\| \leq \|p - x\|, \forall x \neq x_m, x \in I\}. \quad (5.23)$$

The above formula can be used to calculate P_- directly, in which $R(x_m)$ is a polyhedron. However, this formula is not convenient to calculate, since one has to calculate T as well as the union of P_0 and $R(x_m)$. This motivates us to look deep into the relationship between P_- and P_0 . In the following lemma, we present will a simpler formula of P_- , which allows us to calculate it analytically and more efficiently.

Lemma 5.1. $P_- = P_0 \setminus \bigcup_{x \in K} B_{r_p}(x)$ where $B_{r_p}(x)$ denotes the open ball (or disc in \mathbb{R}^2) centered at x with radius r_p .

The proof of Lemma 5.1 is given in the Appendix. From the definition of P_- , it is not surprising to have the inclusion $P_- \subset P_0 \setminus \bigcup_{x \in K} B_{r_p}(x)$. However, the above theorem gives a stronger result that P_- and $P_0 \setminus \bigcup_{x \in K} B_{r_p}(x)$ are identical. This means that the concave spherical patch can be obtained from P_0 by removing the parts intersecting other "nearby" spherical probes centered at SAS intersection points. This lemma also allows us to characterize the singular circular arcs on the concave spherical patch P_- . We propose a theorem of the SES-singularities as following.

Theorem 5.1. *The following statements hold*

- [1] *There can not exist any singularity on a convex spherical SES patch P_+ .*

- [2] On a toroidal patch P_t , two point-singularities occur when the corresponding SAS circular arc has a radius smaller than r_p and they can be computed following the sketch in Figure Figure 13.
- [3] On a concave spherical SES patch P_- , singular arcs occur when P_- does not coincide with the corresponding concave spherical triangle P_0 . Further, these singular arcs form the boundary of P_- that does not belong to the boundary of P_0 .

Proof. First, if x_{ses} is a point on a convex spherical SES patch, then it has a closest point x_{sas} on an spherical SAS patch. Moreover, x_{sas} is the unique closest point to x_{ses} from Theorem 4.1. This, in turn, implies by Corollary 5.1 that x_{ses} can not be a singularity. In consequence, there can not exist any singularity on a convex spherical SES patch P_+ .

Second, if x_{ses} is a point on a toroidal SES patch, then it has a closest point x_{sas} on an SAS circular arc l_m associated with two SAS-spheres S_i and S_j . Moreover, x_{sas} is not unique if and only if x_{ses} belongs to $[c_i, c_j]$ by Theorem 4.2, which happens only when the radius of l_m is smaller than r_p and x_{ses} is one of two cusps on the toroidal SES patch as showed in Figure 13. By Corollary 5.1, two point-singularities on the toroidal patch P_t can only occur when the corresponding SAS circular arc has a radius smaller than r_p .

Third, if x_{ses} is a point on a concave spherical SES patch P_- corresponding to an SAS intersection point x_m , then $x_{sas} = x_m$ is a closest point to x_{ses} . If x_{ses} belongs to the boundary of P_- but not to the boundary of P_0 , then by the formula characterizing P_- in Lemma 5.1 we know that x_{ses} lies on another nearby probe $\partial B_{r_p}(x)$ where $x \in K$ (and thus $x \neq x_m$). In consequence, x is another closest point to x_{ses} implying that x_{ses} is singularity by Corollary 4.1. On the other hand, if $x_{ses} \in P_-$ but does not belong to $\bigcup_{x \in K} B_{r_p}(x)$, then x_{ses} does not lie on any nearby probe and x_{sas} is the unique closest point among all SAS intersection points. Assume by contradiction that there exist another closest point x to x_{ses} on some SAS spherical patch P_m . Since now by Theorem 4.1 the closest point to any point on $(c_i, x]$ on the SAS is unique, this implies that $x_{ses} = c_i$ (because x_m is another closest point). This is however a contradiction since x_{ses} can not coincide with the center of any SAS-sphere as all the VdW-radii are assumed to be positive. Further, assume by contradiction that there exist a closest point x to x_{ses} on some SAS circular arc l_m . Consequently, x_{ses} lies on the corresponding toroidal patch. According to Theorem 4.2, x_{ses} belongs to $[c_i, c_j]$. If $r_p < r_{l_m}$, then x_{ses} can not belong to the SES which is a contradiction. If $r_p \geq r_{l_m}$, then x_{ses} has to be one of the two cusps. In this case, the two ending points of l_m are both closest points to x_{ses} which are also SAS intersection points. This conflicts with the fact that $x_{sas} = x_m$ is the unique closest point among all SAS intersection points. \square

Remark 5.1. In the third case of Theorem 5.1, P_- can be calculated according to Lemma 5.1. It is obvious that P_- does not coincide with P_0 if and only if $P_0 \cap (\bigcup_{x \in K} B_{r_p}(x))$ is nonempty.

Finally, we state a corollary about classifying all points on the SES into four classes according to the number of its closest points on the SAS.

Corollary 5.2. For any point $x_{ses} \in SES$, assume that the number of its closest points on the SAS is N (denoting $N = \infty$ for an infinite number of closest points). Then, there exists four cases:

- [1] $N = 1$: x_{ses} is not a singularity on the SES, and x_{ses} has an unique closest point $\{x_{sas}^1\}$ on the SAS.
- [2] $2 \leq N < \infty$: x_{ses} is a singularity on a concave spherical SES patch, and its closest points $\{x_{sas}^1, \dots, x_{sas}^N\}$ are among the SAS intersection points.

- [3] $N = \infty$: x_{ses} is a singularity on a toroidal patch corresponding to an SAS circular arc (or a complete circle) on which any point is a closest point on the SAS.

5.3 SES-Area and SES-Volume

With the new Voronoi-type diagram as well as the above singularity analysis we can calculate the SES-area and the SES-volume analytically, which shall be explained in the following.

a. SES-Area

In Connolly's paper [7], the presence of singularities on the SES concave spherical patches made it infeasible to calculate the SES-area exactly. The characterization of the singularities carried out earlier in this paper allows us to calculate the area of each SES patch and sum them up to obtain the exact area of the whole SES. To calculate the area of a convex spherical patch P_+ , we use a similar Gauss-Bonnet formula as (4.19):

$$\sum_v \alpha_v + \sum_e k_e |e| + \frac{1}{r_i^2} A_{P_+} = 2\pi\chi, \quad (5.24)$$

where α_v denotes the angle at a vertex v between neighboring circular arcs on the boundary of P_+ , k_e the geodesic curvature of an edge e on the boundary of P_+ , A_{P_+} is the area of P_+ and χ is the Euler characteristic of P_+ .

To calculate the area of a toroidal patch P_t analytically, we consider two cases, and suppose that P_t corresponds to an SAS circular arc l_m with radius r_{l_m} . In the case where $r_{l_m} > r_p$, there will be no singularity on P_t . With the notations introduced in Figure 12, we therefore have the following formula for calculating the area of P_t :

$$A_{P_t} = r_p \beta_m [r_{l_m} (\theta_1 + \theta_2) - r_p (\sin \theta_1 + \sin \theta_2)]. \quad (5.25)$$

In the case where $r_{l_m} \leq r_p$, there are two singular points on P_t . With the notations introduced in Figure 13, we have the following formula for calculating the area of P_t :

$$A_{P_t} = r_p \beta_m [r_{l_m} (\theta_1 + \theta_2 - 2\theta_0) - r_p (\sin \theta_1 + \sin \theta_2 - 2 \sin \theta_0)]. \quad (5.26)$$

To calculate analytically the area of a concave spherical patch P_- , we use the Gauss-Bonnet theorem on the spherical probe again, see Figure 14. In the previous section, we have obtained that $P_- = P_0 \setminus \bigcup_{x \in K} B_{r_p}(x)$, which implies that all information about the boundary of P_- is known. It allows us to apply the Gauss-Bonnet theorem on the spherical probe, to obtain:

$$\sum_v \alpha_v + \sum_e k_e |e| + \frac{1}{r_p^2} A_{P_-} = 2\pi\chi, \quad (5.27)$$

where α_v denotes the angle at a vertex v on the boundary of P_- , k_e the geodesic curvature of an edge e on the boundary of P_- , A_{P_-} is the area of P_- and χ is the Euler characteristic of P_- .

In summary, the area of each SES patch can be calculated independently and analytically, and we can then sum them up to obtain the exact SES-area A_{ses} .

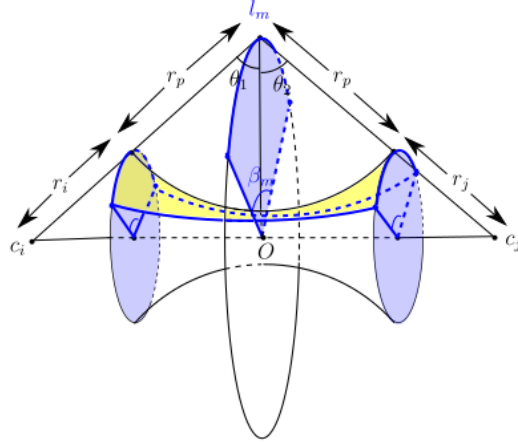


Figure 12: The yellow patch is a toroidal patch P_t on the SES corresponding to an SAS circular arc l_m with the radius $r_{l_m} > r_p$ and the radian β_m . θ_1 denotes the angle between the line connecting c_i with a point on l_m and the disc where l_m lies. Similarly, θ_2 denotes the angle between the line connecting c_j with the same point on l_m and the disc where l_m lies.

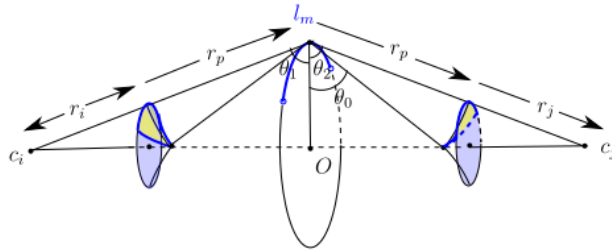


Figure 13: The two yellow parts form a toroidal patch P_t on the SES corresponding to an SAS circular arc l_m with the radius $r_{l_m} < r_p$ and the radian β_m . θ_0 denotes the angle between the line connecting a singularity on P_t with a point on l_m and the disc where l_m lies and θ_1, θ_2 are defined as in Fig. 12.

b. SES-Volume

According to the new Voronoi-type diagram, we can calculate the exact SES-volume. We propose to subtract the volume of the region between the SAS and the SES from the SAS-volume to obtain the SES-volume. This region that needs to be subtracted and which is denoted by R_s can be characterized as below

$$R_s = \{p : -r_p \leq f_{sas}(p) \leq 0\}.$$

From the new Voronoi-type diagram, we decompose R_s into small regions, each of which corresponds to a spherical patch P_m , a circular arc l_m or an intersection point x_m : $R_s \cap R(P_m)$, $R_s \cap R(l_m)$ and $R_s \cap R(x_m)$. The volume of the region $R_s \cap R(P_m)$ is given by

$$V_{R_s \cap R(P_m)} = \frac{1}{3} A_{P_m} (r_i + r_p) \left(1 - \frac{r_i^3}{(r_i + r_p)^3} \right), \quad (5.28)$$

where A_{P_m} is the area of the SAS spherical patch P_m , $r_i + r_p$ is the radius of the corresponding SAS-sphere S_i on which P_m lies. For $R_s \cap R(l_m)$, denote by r_{l_m} the radius of l_m and by β_m the radian of l_m . In the case where $r_{l_m} > r_p$, using the notations of Figure 12, the volume of the region $R_s \cap R(l_m)$ is given by

$$V_{R_s \cap R(l_m)} = \beta_m r_p^2 \left[\frac{r_{l_m}}{2} (\theta_1 + \theta_2) - \frac{r_p}{3} (\sin \theta_1 + \sin \theta_2) \right]. \quad (5.29)$$

In the case where $r_{l_m} \leq r_p$, using the notations of Figure 13, it is given by

$$V_{R_s \cap R(l_m)} = \beta_m r_p^2 \left[\frac{r_{l_m}}{2} (\theta_1 + \theta_2 - 2\theta_0) - \frac{r_p}{3} (\sin \theta_1 + \sin \theta_2 - 2\sin \theta_0) \right] + \frac{1}{3} \beta_m r_{l_m}^2 \sqrt{r_p^2 - r_{l_m}^2}. \quad (5.30)$$

Consider now $R_s \cap R(x_m)$ corresponding to a concave spherical patch P_- . Notice that there might be some flat regions on the boundary of $R_s \cap R(x_m)$, caused by the intersection of the probe $B_{r_p}(x_m)$ and its nearby probes, see Figure 14 (right). Denote by D_i the i -th flat region with the boundary composed of line segments and circular arcs. Furthermore, denote by d_i the distance from x_m to the plane where D_i lies, and by A_{D_i} the area of D_i . Then, the volume of the region $R_s \cap R(x_m)$ can be formulated as:

$$V_{R_s \cap R(x_m)} = \frac{1}{3} A_{P_-} r_p + \sum_i \frac{1}{3} A_{D_i} d_i, \quad (5.31)$$

where, A_{P_-} is the area of the concave spherical SES patch P_- . Finally, by summing up the volume of each subtracted region, we obtain the subtracted volume as following:

$$V_{R_s} = \sum_{\xi=P_m, l_m, x_m} V_{R_s \cap R(\xi)}. \quad (5.32)$$

Therefore, the SES-volume denoted by V_{ses} is equal to $V_{sas} - V_{R_s}$.

6 Construction of Molecular Surfaces

In the above sections, we have defined and analyzed the cSAS and the eSAS, as well as the cSES and the eSES. However, all work is based on the explicit knowledge of the components of these molecular surfaces. In this section, we will present a method of constructing the cSAS and

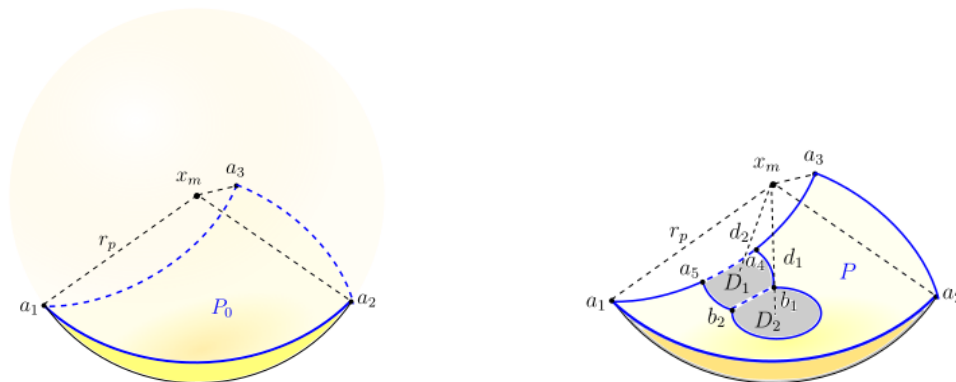


Figure 14: On the left, the concave spherical triangle P_0 with vertices (a_1, a_2, a_3) corresponds to an intersection point x_m . In the case where P_- coincide with P_0 , there will be no singularity on the concave spherical patch. On the right, the concave spherical patch P_- does not coincide with P_0 and there are singular circular arcs as parts of its boundary. The vertices of P_- are $(a_1, a_2, a_3, a_4, b_1, b_2, a_5)$. The two flat grey regions D_1 and D_2 are formed by the intersection of P_0 with two other nearby spherical probes. These two regions have the boundaries composed of line segments and circular arcs.

Molecule	A_{cses}	A_{eses}	$\frac{\Delta A_{ses}}{A_{eses}}$	A_{csas}	A_{esas}	$\frac{\Delta A_{sas}}{A_{esas}}$
1ETN	9.422583e+02	9.422583e+02	1.206536e-16	1.382551e+03	1.382551e+03	0
1B17	3.399840e+03	3.358776e+03	-1.222581e-02	4.296868e+03	4.296137e+03	-1.701293e-04
101M	7.858419e+03	7.186689e+03	-9.346864e-02	8.625944e+03	8.573658e+03	-6.098466e-03
Molecule	V_{cses}	V_{eses}	$\frac{\Delta V_{ses}}{V_{eses}}$	V_{csas}	V_{esas}	$\frac{\Delta V_{sas}}{V_{esas}}$
1ETN	1.510239e+03	1.510239e+03	-1.505548e-16	3.249583e+03	3.249583e+03	0
1B17	8.090117e+03	8.117766e+03	3.405988e-03	1.394413e+04	1.394415e+04	1.620417e-06
101M	2.319527e+04	2.379511e+04	2.520849e-02	3.581084e+04	3.581810e+04	2.027866e-04

Table 1: Different molecular areas (in \AA^2 , top) and volumes (in \AA^3 , bottom) for three molecules (1ETN, 1B17, 101M from the protein data bank <http://www.rcsb.org/pdb/home/home.do>) where we use the notation $\Delta A_{ses} = A_{eses} - A_{cses}$ and $\Delta A_{sas} = A_{esas} - A_{csas}$ resp. $\Delta V_{ses} = V_{eses} - V_{cses}$ and $\Delta V_{sas} = V_{esas} - V_{csas}$. The probe radius r_p is fixed to be 1.5\AA .

the eSAS using a binary tree to construct its spherical patches. After that, we will give a brief construction strategy of the cSES and eSES based on the construction of the cSAS and the eSAS. The construction of molecular surfaces ensures that our previous analysis is feasible.

6.1 Construction of the cSAS and the eSAS

To start the construction, we need some quantities for representing different components of the SAS. First, an intersection point will be represented by its coordinate in \mathbb{R}^3 and an identifier. Second, to represent a circular arc, we use its starting and ending intersection points (resp. the identifiers), its radius, center and radian as well as an identifier. Finally, to represent a spherical patch, we use the SAS-sphere on which it lies on and the identifiers of all circular arcs forming its boundary. Then, we propose to construct the SAS in five basic steps as below:

- 1) Compute the set of all intersection points $\{x_1, \dots, x_{m_1}\}$, denoted by I .
- 2) Calculate each SAS circular arc or circle l_m associated with some S_i and S_j . For each SAS circular arc or circle, we record the information, including the center, the radius, the radian, the corresponding two SAS spheres, the identifiers of the starting and ending intersection points. Notice that each circular arc connects two intersection points.
- 3) Construct all loops on each SAS sphere S_i , which also form the boundaries of SAS spherical patches on S_i . Notice that each loop is composed of circular arcs, or a complete circle. We start from a circular arc on S_i , find another arc connecting this arc, add it into the loop, and repeat this until we finally obtain a complete loop. The k -th loop on the i -th SAS sphere is denoted by \mathcal{L}_k^i .
- 4) Construct all spherical patches on each SAS sphere S_i . Since the boundary of a spherical patch on S_i is composed by one or several loops on S_i , we can use the identifiers of these loops to represent a spherical patch. Denote by P_k^i the k -th spherical patch on S_i . The difficulty lies on determining whether two loops on S_i belong to the boundary of a common spherical patch or not. This final question will be discussed in the next section.
- 5) Finally, we should distinguish the cSAS and the eSAS. The cSAS is just the set of all above-constructed SAS spherical patches. To construct the eSAS, we say that two spherical patches P_k^i and P_l^j are neighbors if they have a common circular arc or circle on their boundaries. Then, we start our construction of the eSAS, by mapping a faraway point p_∞ onto an SAS spherical patch, which is the initial patch on the eSAS. Then, we add the neighboring spherical patches into the eSAS one by one, to finally obtain the whole eSAS.

6.2 Binary Tree to Construct Spherical Patches

In the above construction process, there remains a problem of classifying the loops on an SAS-sphere into several parts, such that each part forms the boundary of a spherical patch. To do this, we need to determine whether two loops on the SAS-sphere belong to the boundary of a same spherical patch or not. Note that two different loops won't cross each other but can have common vertices. We propose to construct a binary tree whose leaves are the different spherical patches.

Given a loop \mathcal{L} on a fixed SAS-sphere S_i , \mathcal{L} divides the sphere into two open parts and it is composed of circular arcs formed by the intersection of S_i and other SAS-spheres. We call the open

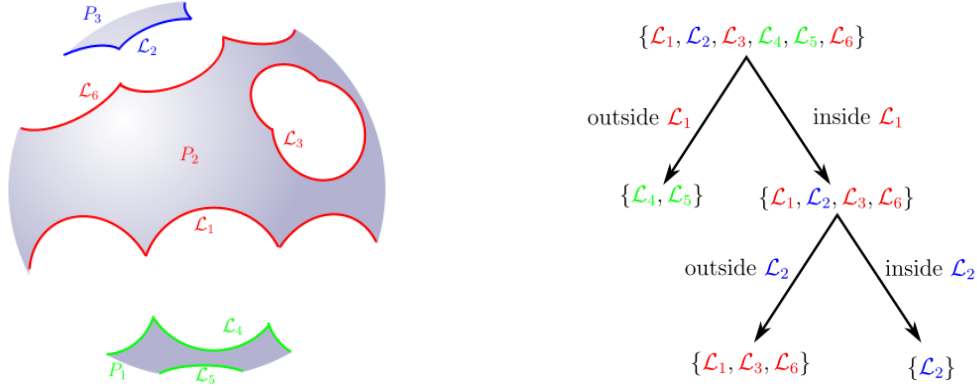


Figure 15: On the left is a brief schematic of an SAS-sphere and the loops on it. There are six loops on the SAS-sphere $\{\mathcal{L}_1, \mathcal{L}_2, \mathcal{L}_3, \mathcal{L}_4, \mathcal{L}_5, \mathcal{L}_6\}$, and three spherical patches with the boundaries formed by two loops in green $\{\mathcal{L}_4, \mathcal{L}_5\}$, three loops in red $\{\mathcal{L}_1, \mathcal{L}_3, \mathcal{L}_6\}$ and one loop (circle) in blue $\{\mathcal{L}_2\}$ respectively. The tree on the right illustrates the corresponding binary tree whose leaves identify the boundaries of three different spherical patches.

part of S_i which is not hidden by those other SAS-spheres as the interior of \mathcal{L} , denoted by \mathcal{L}° , while the other open part as the exterior of \mathcal{L} , denoted by \mathcal{L}^c . We say that another loop \mathcal{L}' on S_i is inside \mathcal{L} if $\mathcal{L}' \in \overline{\mathcal{L}^\circ}$, where $\overline{\mathcal{L}^\circ} = \mathcal{L} \cup \mathcal{L}^\circ$ is the closed hull of \mathcal{L}° on S_i . Notice that each loop \mathcal{L} being part of the boundary of a spherical patch contains all the other loops that belong to the boundary of the same patch. By testing if a loop \mathcal{L}' on S_i is inside the loop \mathcal{L} , we can classify all loops on S_i into two parts: the loops inside \mathcal{L} (including \mathcal{L} itself) and the remaining loops outside \mathcal{L} . We do this division repeatedly until each loop is tested which results in a binary tree.

To better understand this process, let's see the example of Figure 15. On an SAS-sphere S_i , there are six loops $\{\mathcal{L}_1, \mathcal{L}_2, \mathcal{L}_3, \mathcal{L}_4, \mathcal{L}_5, \mathcal{L}_6\}$ forming three spherical patches $\{P_1, P_2, P_3\}$ with green, red and blue boundaries. The leaves of the binary tree in Figure 15 represent the boundary of the three spherical patches. To construct the tree, consider all loops $\{\mathcal{L}_1, \mathcal{L}_2, \mathcal{L}_3, \mathcal{L}_4, \mathcal{L}_5, \mathcal{L}_6\}$ and test with \mathcal{L}_1 , to divide into the set of loops inside \mathcal{L}_1 ($\{\mathcal{L}_1, \mathcal{L}_2, \mathcal{L}_3, \mathcal{L}_6\}$) and the set of the remaining loops outside \mathcal{L}_1 ($\{\mathcal{L}_4, \mathcal{L}_5\}$). Then, we test with \mathcal{L}_2 , to find that \mathcal{L}_2 is inside itself, while $\{\mathcal{L}_1, \mathcal{L}_3, \mathcal{L}_6\}$ are outside, which implies that \mathcal{L}_2 itself forms the boundary of a spherical patch. Afterwards, we find that $\{\mathcal{L}_1, \mathcal{L}_6\}$ are both inside \mathcal{L}_3 by testing with \mathcal{L}_3 and that $\{\mathcal{L}_1, \mathcal{L}_3\}$ are inside \mathcal{L}_6 by testing with \mathcal{L}_6 . This implies that $\{\mathcal{L}_1, \mathcal{L}_3, \mathcal{L}_6\}$ form the boundary of the second spherical patch, as these three loops are inside each other. Finally, we test respectively with \mathcal{L}_4 and \mathcal{L}_5 to find that they are inside each other and they form the boundary of the last spherical patch.

6.3 Interior of a Loop

Let \mathcal{L}' and \mathcal{L} be two loops on S_i . It is left to explain how to test whether \mathcal{L}' is inside \mathcal{L} or not. We assume that \mathcal{L} is composed by n circular arcs which are formed by the intersection of S_i and other SAS-spheres S'_1, \dots, S'_n . Denote all intersection circles by C_1, \dots, C_n , where $C_j = S_i \cap S'_j$. The corresponding SAS-balls to S'_1, \dots, S'_n are denoted by B'_1, \dots, B'_n . Since \mathcal{L}' and \mathcal{L} do not cross each other, we can determine if the loop \mathcal{L}' is inside \mathcal{L} or not by testing whether a particular point

$x \in \mathcal{L}'$ is inside \mathcal{L} or not. We denote by x_k ($1 \leq k \leq n$) the closest point on C_k to x , which can be analytically given. Notice that x_k has the smallest Euclidean distance in \mathbb{R}^3 from x to any point on C_k , which is equivalent to that the shortest path on S_i from x to C_k which ends at x_k . For all circles C_k , $k = 1, \dots, n$, we can then find the circle C_{k_0} with the minimum path length on S_i from x to C_k . The closest point on C_{k_0} to x is thus denoted by x_{k_0} . With these notations, the following lemma is proposed to test whether x is inside \mathcal{L} or not, note that $\mathcal{L}' \cap \bigcup_{j=1}^n B'_j = \emptyset$.

Lemma 6.1. *Given an arbitrary point $x \in S_i \setminus \bigcup_{j=1}^n B_j$, x is inside \mathcal{L} if and only if $x_{k_0} \in \mathcal{L}$.*

Proof. We first prove the sufficiency. Assume that x is inside \mathcal{L} , i.e. $x \in \overline{\mathcal{L}^\circ} = \mathcal{L}^\circ \cup \mathcal{L}$. Assume by contradiction that $x_{k_0} \in C_{k_0}$ does not belong to \mathcal{L} . Then, since $C_{k_0} \subset \mathcal{L} \cup \mathcal{L}^c$ it follows that $x_{k_0} \in \mathcal{L}^c$. Then, the shortest path on S_i from $x \in \mathcal{L}^\circ$ to $x_{k_0} \in \mathcal{L}^c$ must cross \mathcal{L} . In consequence, the intersection point between \mathcal{L} and the shortest path on S_i has a smaller path length to x than x_{k_0} does, which is a contradiction. Therefore there holds that $x_{k_0} \in \mathcal{L}$.

Second, we prove the necessity. Assume that $x_{k_0} \in \mathcal{L}$. By contradiction again, we assume that x is not inside \mathcal{L} , i.e. $x \in \mathcal{L}^c$, which yields that $x \in \Omega := \mathcal{L}^c \setminus \bigcup_{j=1}^n B_j$ from the lemma's condition. Then, the shortest path on S_i between $x \in \Omega$ and $x_{k_0} \notin \Omega$ must cross $\Gamma = \partial\Omega$. In consequence, the intersection point between Γ and the shortest path on S_i has a smaller path length to x than x_{k_0} does, which is a contradiction. Therefore, x lies inside \mathcal{L} . \square

6.4 Construction of the cSES and the eSES

The SES (both the cSES and the eSES) has been divided into three types of patches: convex spherical patches, toroidal patches and concave spherical patches. With the construction of the cSAS and the eSAS, the patches of the cSES and the eSES can be distinguished since each patch corresponds to a component of the SAS. Furthermore, a patch on the SES will be represented by its boundary composed of circular arcs, where a circular arc is represented by its starting and ending points, its radius, center and radian. Consequently, a convex spherical patch on the SES can be obtained directly by shrinking its corresponding SAS-patch from the SAS-sphere to the VdW-sphere. A toroidal patch on the SES can also be given considering two cases respectively showed in Figure 12 and Figure 13 (see the paper [7]). Finally, we can compute every concave toroidal patch from the formula in Lemma 5.1, using a binary tree for its corresponding spherical probe similar to the one for an SAS-sphere S_i .

7 Conclusion

In this paper, based on three equivalence statements and a new Voronoi-type diagram, an analytical and also computable implicit function of the SES has been provided. Furthermore, all SES patches including SES-singularities can be characterized and computed according to Lemma 5.1 and Theorem 5.1. Consequently, different molecular areas and volumes can be calculated analytically with explicit formulas. In addition, we have also proposed the concept of the cSAS and the eSAS (as well as the cSES and the eSES), considering the possible inner holes inside a solute molecule or not. Finally, a corresponding method to construct (or distinguish) the cSAS and the eSAS has been given, with the use of a binary tree. In summary, the molecular surfaces have been analytically characterized (especially the SES), which allows to do more accurate calculation in solvation models associated with different molecular cavities.

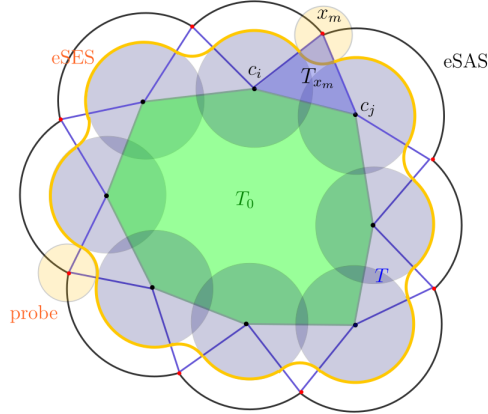


Figure 16: A 2D schematics of the two different polygons in the eSAS-cavity of an artificial molecule for the proof of Lemma A.1. T_{x_m} is the triangle with three vertices (x_m, c_i, c_j) and the polygon in green is the reduced polygon T_0 .

Acknowledgments

The authors thank Pascal Frey and Yvon Maday for the fruitful discussion.

Appendix: Proof of Lemma 5.1

First, we provide a lemma about the geometric relationship between P_0 and $T = R(I)$ as following.

Lemma A.1. *There holds that $P_0 \setminus \bigcup_{x \in K} B_{r_p}(x) \subset T$, where $T = R(I)$ is the closed region composed of polyhedrons in the SAS-cavity.*

Proof. We first recall an equivalence relationship for three sets A , B and C :

$$A \setminus B \subset C \iff A \subset B \cup C \iff A \setminus C \subset B.$$

In consequence, to prove the lemma is equivalent to prove that $P_0 \setminus T \subset \bigcup_{x \in K} B_{r_p}(x)$. For simplicity, we only give the proof for the case of the eSAS in \mathbb{R}^2 . There is no essential additional difficulty for the proof in \mathbb{R}^3 . We define another polygon called the reduced polygon T_0 contained in T (see Figure 16), which is obtained by removing from T those vertices which are SAS intersection points, so that only the centers of the SAS-balls are left as vertices. In consequence, we have a simple relationship $T = (\bigcup_{x_m \in I} T_{x_m}) \cup T_0$, in which T_{x_m} is the triangle with the three vertices x_m , c_i and c_j . Each edge of T_0 is associated with an SAS intersection point.

With the above notations, three cases will be discussed as following:

- a) $P_0 \subset T_{x_m}$: Since $T_{x_m} \subset T$ implies that $P_0 \setminus T = \emptyset$, this is a trivial case.
- b) $P_0 \subset T_{x_m} \cup T_0$: Since $T_{x_m} \cup T_0 \subset T$ implies that $P_0 \setminus T = \emptyset$, this is also a trivial case.

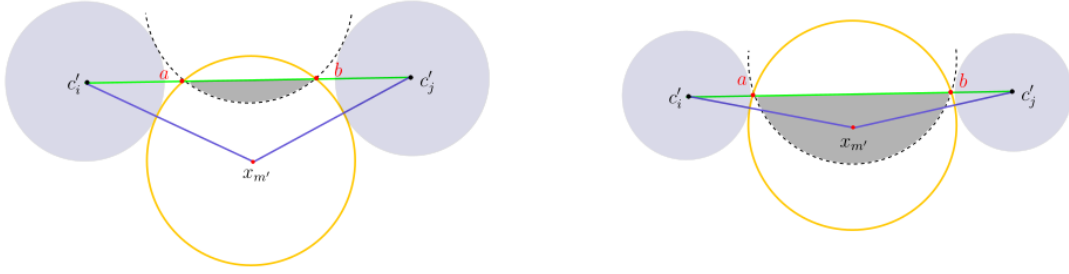


Figure 17: 2D schematics of two cases where $P_0 \cap T_{x_{m'}} \neq \emptyset$ with $x_{m'}$ being an SAS intersection point different from x_m . The green segment $[c'_i, c'_j]$ is an edge of T_0 and a and b are the two intersection points between the circle $\partial B_{r_p}(x_{m'})$ and the segment $[c'_i, c'_j]$. The grey region is the region where P_0 can possibly appear outside T_0 that may be included in the triangle $\triangle x_{m'} c'_i c'_j$ (left) or not (right).

- c) $\exists x_{m'} \neq x_m$ s.t. $P_0 \cap T_{x_{m'}} \neq \emptyset$: Figure 17 gives the schematics of the region (in grey) where P_0 can possibly appear outside T_0 . If this region is included in $T_{x_{m'}}$, the proof is again trivial. If parts of this region lies outside $T_{x_{m'}}$, then this region is include by the probe $B_{r_p}(x_{m'})$ by symmetry. In consequence, all such regions can be covered by the corresponding spherical probes, implying that $P_0 \setminus T \subset \bigcup_{x \in K} B_{r_p}(x)$.

□

With the above lemma, we can now prove Lemma 5.1. According to the definition of K , it accounts for all SAS intersection points that might intersect $B_{r_p}(x_m)$ and thus $P_0 \setminus \bigcup_{x \in K} B_{r_p}(x) = P_0 \setminus \bigcup_{x \in I} B_{r_p}(x)$. We first observe that

$$P_0 \setminus B_{r_p}(x) = P_0 \cap (B_{r_p}(x))^c = P_0 \cap \{p : \|p - x_m\| \leq \|p - x\|\}, \quad \forall x \neq x_m, \quad (\text{A.33})$$

and therefore we obtain that

$$\begin{aligned} P_0 \setminus \bigcup_{x \in K} B_{r_p}(x) &= \left(P_0 \setminus \bigcup_{x \in K} B_{r_p}(x) \right) \cap T \\ &= \bigcap_{x \in I} (P_0 \setminus B_{r_p}(x)) \cap T \\ &= P_0 \cap T \cap \{p : \|p - x_m\| \leq \|p - x\|, \forall x \neq x_m, x \in I\} \\ &= P_- . \end{aligned} \quad (\text{A.34})$$

In the above, the first equality results from Lemma A.1, the third one from equation (A.33) and the last one from (5.23).

References

- [1] Franz Aurenhammer. Power diagrams: properties, algorithms and applications. *SIAM Journal on Computing*, 16(1):78–96, 1987.

- [2] David Avis, Binay K Bhattacharya, and Hiroshi Imai. Computing the volume of the union of spheres. *The Visual Computer*, 3(6):323–328, 1988.
- [3] Ján Buša, Jozef Džurina, Edik Hayryan, Shura Hayryan, Chin-Kun Hu, Ján Plavka, Imrich Pokorný, Jaroslav Skřivánek, and Ming-Chya Wu. Arvo: a fortran package for computing the solvent accessible surface area and the excluded volume of overlapping spheres via analytic equations. *Computer physics communications*, 165(1):59–96, 2005.
- [4] Eric Cancès, Yvon Maday, and Benjamin Stamm. Domain decomposition for implicit solvation models. *The Journal of chemical physics*, 139(5):054111, 2013.
- [5] Frederic Cazals, Harshad Kanhere, and Sebastien Lorient. Computing the volume of a union of balls: a certified algorithm. *ACM Transactions on Mathematical Software (TOMS)*, 38(1):3, 2011.
- [6] Calvin Chen and George Makhatadze. Proteinvolume: calculating molecular van der waals and void volumes in proteins. *BMC Bioinformatics*, 16(1):101, 2015.
- [7] M. L. Connolly. Analytical molecular surface calculation. *Journal of Applied Crystallography*, 16(5):548–558, Oct 1983.
- [8] Manfredo Perdigao Do Carmo and Manfredo Perdigao Do Carmo. *Differential geometry of curves and surfaces*, volume 2. Prentice-hall Englewood Cliffs, 1976.
- [9] Robert Lewis (Scot) Drysdale, III. *Generalized Voronoi Diagrams and Geometric Searching*. PhD thesis, Stanford University, Stanford, CA, USA, 1979. AAI7917225.
- [10] Herbert Federer. The gauss-green theorem. *Transactions of the American Mathematical Society*, pages 44–76, 1945.
- [11] Daniel Kauker, Michael Krone, Alexandros Panagiotidis, Guido Reina, and Thomas Ertl. Rendering molecular surfaces using order-independent transparency. In *Proceedings of the 13th Eurographics Symposium on Parallel Graphics and Visualization*, pages 33–40. Eurographics Association, 2013.
- [12] Byungkook Lee and Frederic M Richards. The interpretation of protein structures: estimation of static accessibility. *Journal of molecular biology*, 55(3):379–IN4, 1971.
- [13] Filippo Lipparini, Benjamin Stamm, Eric Cancès, Yvon Maday, and Benedetta Mennucci. Fast domain decomposition algorithm for continuum solvation models: Energy and first derivatives. *Journal of Chemical Theory and Computation*, 9(8):3637–3648, 2013.
- [14] Julius Parulek and Ivan Viola. Implicit representation of molecular surfaces. In *Pacific Visualization Symposium (PacificVis), 2012 IEEE*, pages 217–224. IEEE, 2012.
- [15] Christian S Pomelli and Jacopo Tomasi. Defpol: New procedure to build molecular surfaces and its use in continuum solvation methods. *Journal of computational chemistry*, 19(15):1758–1776, 1998.
- [16] Anthony K Rappé, Carla J Casewit, KS Colwell, WA Goddard Iii, and WM Skiff. Uff, a full periodic table force field for molecular mechanics and molecular dynamics simulations. *Journal of the American Chemical Society*, 114(25):10024–10035, 1992.

- [17] Frederic M Richards. Areas, volumes, packing and protein structure. *Annual Review of Biophysics and Bioengineering*, 6:151–176, 1977.
- [18] Timothy J Richmond. Solvent accessible surface area and excluded volume in proteins: Analytical equations for overlapping spheres and implications for the hydrophobic effect. *Journal of molecular biology*, 178(1):63–89, 1984.
- [19] Michel F Sanner, Arthur J Olson, and Jean-Claude Spehner. Reduced surface: an efficient way to compute molecular surfaces. *Biopolymers*, 38(3):305–320, 1996.
- [20] Jacopo Tomasi, Benedetta Mennucci, and Roberto Cammi. Quantum mechanical continuum solvation models. *Chemical reviews*, 105(8):2999–3094, 2005.
- [21] Luiz Velho, Jonas Gomes, and Luiz H de Figueiredo. *Implicit objects in computer graphics*. Springer Science & Business Media, 2002.